

Review

Modelling of the ventricular conduction system

K.H.W.J. Ten Tusscher*, A.V. Panfilov

Department of Theoretical Biology, Utrecht University, Padualaan 8, 3584 CH Utrecht, The Netherlands

Available online 24 August 2007

Abstract

The His–Purkinje conduction system initiates the normal excitation of the ventricles and is a major component of the specialized conduction system of the heart. Abnormalities and propagation blocks in the Purkinje system result in abnormal excitation of the heart. Experimental findings suggest that the Purkinje network plays an important role in ventricular tachycardia and fibrillation, which is the major cause of sudden cardiac death.

Nowadays an important area in the study of cardiac arrhythmias is anatomically accurate modelling. The majority of current anatomical models have not included a description of the Purkinje network. As a consequence, these models cannot be used to study the important role of the Purkinje system in arrhythmia initiation and maintenance.

In this article we provide an overview of previous work on modelling of the Purkinje system and report on the development of a His–Purkinje system for our human ventricular model. We use the model to simulate the normal activation pattern as well as abnormal activation patterns resulting from bundle branch block and bundle branch reentry. © 2007 Elsevier Ltd. All rights reserved.

Keywords: His–Purkinje system; Ventricular arrhythmias; Mathematical model; Simulation studies

Contents

1. Introduction	153
2. Existing His–Purkinje system models	154
3. Existing Purkinje cell models	156
4. Methods	157
4.1. Electrophysiological model	157
4.2. Human ventricular anatomy and anisotropy	157
4.3. Numerical integration	158
4.4. Implementation	159
4.5. Development of the His–Purkinje conduction system	159
5. Results	161
5.1. Normal activation sequence	161
5.2. Bundle branch block	163
5.3. Bundle branch reentry	164

*Tel.: + 31 30 2533695; fax: + 31 30 2513655.

E-mail address: khwtjuss@hotmail.com (K.H.W.J.T. Tusscher).

6. Discussion	166
6.1. Limitations.	166
Acknowledgement	167
References	167

1. Introduction

The coordinated contraction of the heart is regulated by the specialized electrical conduction system of the heart (Eckert et al., 1988; Berne and Levy, 1993; Silverman et al., 2006). The main parts of this conduction system are the sino-atrial (SA) node, Bachmann's bundle, atrio-ventricular (AV) node, the His bundle, Tawara branches and Purkinje fibres. The SA node, located in the upper right atrium, is the primary pacemaker of the heart, automatically generating electrical pulses. These electrical pulses spread as waves of electrical excitation over the atria, with the Bachmann's bundle ensuring fast propagation toward the left atrium, leading to atrial contraction. The atria and ventricles are electrically isolated from each other except for the region of the AV node via which the excitation passes to ventricles. The speed of propagation in the AV node is slow, causing a delay in the passage of the electrical wave from the atria to the ventricles, ensuring that the ventricles contract after the atria. In the ventricles the excitation spreads at a high speed from the AV node through the His-bundle, left and right Tawara branches and Purkinje fibres. The Purkinje fibres are electrically connected to the ventricular muscle at certain insertion sites, from which the wave enters the ventricular wall, leading to ventricular excitation and contraction.

The above described pattern of excitation corresponds to the normal sequence of cardiac activation. Abnormalities in this pattern may lead to cardiac arrhythmias. They may occur in any of the elements of the conduction pathway. An example of an abnormal excitation pattern involving the His–Purkinje system is left or right bundle branch block, which leads to indirect, delayed activation of the right or left ventricle, respectively (Imanishi et al., 2006; Fantoni et al., 2005; Niu et al., 2006). Another example is bundle branch reentry, where partial block in one of the bundle branches leads to occasional unidirectional block and a macro reentry through the full His–Purkinje system, giving rise to ventricular tachycardia (Caceres et al., 1989; Mazur et al., 2005). In addition, the His–Purkinje system is considered to play an important role in the development and/or maintenance of some types of ventricular tachycardia and fibrillation in which repeated subendocardial focal activity, presumably of Purkinje origin, is observed to occur (Pogwizd and Corr, 1992; Chung et al., 1997; Pogwizd et al., 1998; Arnar et al., 1997, 2001; Arnar and Martins, 2002). The source of this Purkinje focal activity has been hypothesized to be either abnormal automaticity of the Purkinje fibres, or triggered activity, i.e. early afterdepolarizations (EADs) and delayed afterdepolarizations (DADs), or (micro)reentry (Arnar et al., 1997, 2001; Pogwizd et al., 1998; Xing and Martins, 2004). However, so far, it has not been clearly established which of these mechanisms actually occur, and under what kind of circumstances.

Since the His–Purkinje system plays such an important role in both normal ventricular excitation and life threatening ventricular arrhythmias, modelling of the His–Purkinje system is essential for a realistic ventricle model of the heart. In this article we will review existing models of the His–Purkinje system and present the development of a His–Purkinje model for our human ventricles model. The model is based both on anatomical knowledge of the His–Purkinje system (Tawara, 2000; Keith and Flack, 1906; Spach et al., 1963; James and Sherf, 1971; James et al., 1974; Massing and James, 1976) and the sites of earliest activation and normal activation sequence as reported by Durrer et al. (1970). Anatomy and conductance parameters of the His–Purkinje system were iteratively adjusted to correctly reproduce the Durrer et al. (1970) activation data. The electrophysiological behaviour of individual ventricular and Purkinje cells is modelled using our detailed human ventricular cell model (Ten Tusscher et al., 2004; Ten Tusscher and Panfilov, 2006), with a few modifications to account for differential Purkinje cell behaviour.

We show that our His–Purkinje–ventricles model produces an activation sequence that agrees well with the activation data from Durrer et al. (1970). We furthermore demonstrate realistic activation sequences for left and right bundle branch blocks. Finally, we use the developed model to study the occurrence of bundle branch

reentry. We show that significant delays in His–Purkinje and interventricular conduction are needed to allow for an effective path length that is long enough to support sustained reentry.

2. Existing His–Purkinje system models

An extensive amount of modelling has already been done on reproducing (ab)normal activation sequences and incorporating a His–Purkinje system in 3D ventricular models. Here we review several important models that have been developed over the years.

Early 3D ventricular models, like the one constructed by Miller and Geselowitz (1978a,b) did not incorporate a specialized conduction system, but used the sites of earliest activation as measured by Durrer et al. (1970) to initiate activation sequences. The Miller–Geselowitz model consisted of approximately 4000 grid points, with a spatial resolution of 3.75–4.64 mm (depending on the direction), and was used to reproduce the electrocardiogram (ECG) generated by normal activation and activation under local ischemia.

Probably the first 3D ventricular model incorporating a His–Purkinje system is the model developed by Aoki, Wei and co-workers (Aoki et al., 1986, 1987; Wei et al., 1987, 1990; Okazaki et al., 1998) (Fig. 1A). They constructed an anatomically based human 3D whole heart model, including atria, ventricles and a specialized conduction system. The model consisted of 50,000 elements and had a spatial resolution of 1.5 mm. The early version of the model contained no fibre direction anisotropy, this was included in a later version of the model (Wei et al., 1995). The model contained a simple His–Purkinje system, with His bundle, left and right bundle branches and Purkinje fibres, consisting of a few hundred elements. Excitable behaviour of the cells was modelled with a rule based cellular automata approach. The model was used to verify the normal activation

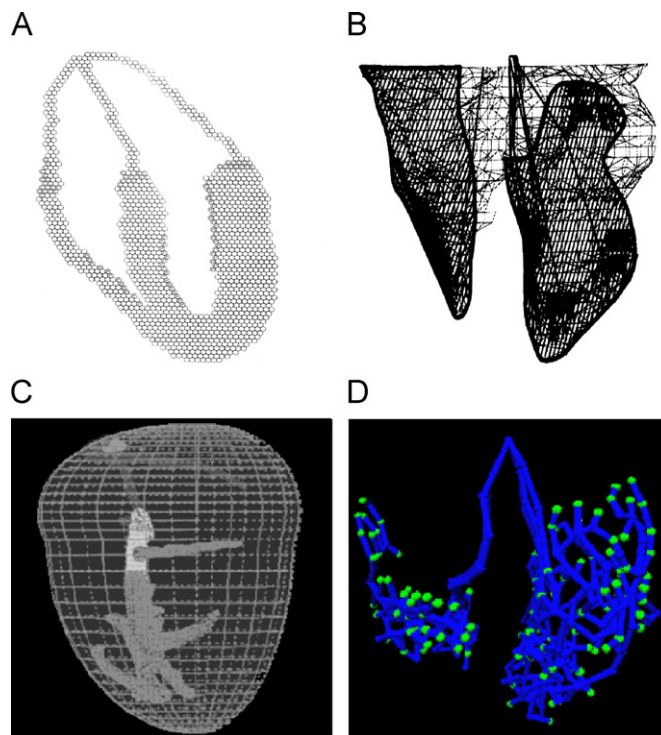


Fig. 1. (A) Transversal cross-section through the heart model by Aoki, Wei and co-workers (Aoki et al., 1986, 1987; Wei et al., 1987, 1990; Okazaki et al., 1998). The letter P denotes cells that are part of the Purkinje system. Reprinted with permission from the *Journal of Electrocardiology* (Wei et al., 1990). (B) Heart and His–Purkinje system in the model by Lorange and Gulrajani (1993). Reprinted with permission from the *Journal of Electrocardiology* (Lorange and Gulrajani, 1993). (C) Heart and specialized conduction system developed by Siregar et al. (1998). Reprinted with permission from *Computers and Biomedical Research* (Siregar et al., 1998). (D) Purkinje system developed by Simelius et al. (2001). In blue are the Purkinje cables, in green the Purkinje–muscle insertion points. Reprinted with permission from the *International Journal of Bioelectromagnetism* (Simelius et al., 2001).

sequence (Aoki et al., 1986, 1987), and reproduce ECGs generated by bundle branch block (Aoki et al., 1987) and Wolff–Parkinson–White syndrome (Wei et al., 1987, 1990), and, more recently, to simulate ventricular fibrillation (Okazaki et al., 1998).

Abboud et al. (1991) constructed a finite element ventricles model including a His–Purkinje system. The ventricles were modelled as two joined spheroids, whereas the Purkinje system was modelled as an idealized, self-similar fractal tree. The model contained around 500,000 elements and had a spatial resolution of 3–4 mm, depending on the direction. Cardiac depolarization was described using a rule based cellular automata approach. The model was used to simulate the ECG's QRS complex resulting from activation under normal conditions and local ischemia. A very similar approach was used by Adam (1991).

Pollard and Barr (1990, 1991) developed a detailed fine grained model of the human His–Purkinje system consisting of 33,000 elements, which, however, was not incorporated in a ventricular anatomy. They modelled only the upstroke phase of cardiac excitation with the Ebihara–Johnson sodium current formulation. The Purkinje model was validated against activation time data.

Lorange and co-workers (Lorange and Gulrajani, 1993; Lorange et al., 1993; Xu et al., 1996; Dube et al., 1996) developed and incorporated a schematic His–Purkinje system in their human ventricles model. The ventricles model consisted of approximately 250,000 nodes, with spatial resolutions of 1 mm, and contained a stylized fibre direction field. The His–Purkinje model consisted of cables for the common His bundle and for the left and right bundle branches, the distal Purkinje network was represented as a sheet of conduction tissue containing the Purkinje muscle junction (PMJ) sites (Fig. 1B). The model was used to simulate activation patterns under normal conduction, conduction blocks, ectopic beats and ischemia.

Berenfeld and co-workers (Berenfeld and Abboud, 1996; Berenfeld and Jalife, 1998) proposed an anatomically based His–Purkinje system for their model of the canine ventricles. The ventricular model had a spatial resolution of 1 mm (145,000 grid points) and cardiac excitation properties were modelled with FitzHugh–Nagumo type dynamics. The Purkinje system consisted of a total of 4539 elements, with 214 elements connecting the Purkinje system to the ventricles via a total of around 70 PMJs. The model was used to simulate the normal cardiac excitation sequence. In addition, the model was used to simulate micro reentry within the Purkinje system giving rise to a ventricular tachyarrhythmia.

Siregar et al. (1998) developed a model of the complete human heart, including atria, ventricles, SA and AV nodes and specialized conduction system. The model contained a simplified conduction system that contains a few branches connecting the sites of earliest activation as reported by Durrer et al. (1970) directly to the Tawara branches and His bundle (Fig. 1C). The model contained an idealized muscle fibre field for anisotropic propagation. The spatial resolution and number of nodes in the model can be varied, with a maximum of around 400,000 nodes. Excitable behaviour of the cardiac cells was modelled using a rule based cellular automata approach.

Simelius et al. (2001) incorporated a detailed anatomically based His–Purkinje system in their human ventricles model (Fig. 1D). The model had a spatial resolution of 0.5 mm and consisted of around 1.8×10^6 elements. Excitable behaviour of the individual cardiac cells was modelled using cellular automata. The model was used to simulate the normal excitation sequence of the heart and the ECG and body surface maps this results in.

Recently, Vigmond and Clements (2007) developed an anatomically based Purkinje system for the San Diego rabbit ventricles model. The Purkinje system consisted of 851 node points with a spatial resolution of 0.25–0.5 mm. Excitable behaviour of the Purkinje system was modelled using the DiFrancesco and Noble (1985) model. A cubic Hermite finite elements bidomain modelling approach was used to ensure current conservation on Purkinje cable bifurcation and merging points. The model was used to simulate the normal ventricular activation sequence and to study the potential occurrence of sawtooth effects in the Purkinje system under external stimulation.

The reviewed His–Purkinje models differ in anatomical detail, spatial resolution and the approach used to model cardiac cellular excitation. With respect to anatomy, all models reviewed included a common His bundle and the left and right bundle branches. However, in most models the distal Purkinje network was not based on anatomical data but was described either as a few simple branches (Aoki et al., 1986, 1987; Wei et al., 1987, 1990; Okazaki et al., 1998; Siregar et al., 1998), or as a self-similar fractal tree (Abboud et al., 1991) or as a conductive tissue sheet containing insertions sites (Lorange and Gulrajani, 1993; Lorange et al., 1993;

Xu et al., 1996; Dube et al., 1996). Only the models by Berenfeld and co-workers, Simelius et al., and Clements and Vigmond (Berenfeld and Abboud, 1996; Berenfeld and Jalife, 1998; Simelius et al., 2001; Clements and Vigmond, 2005) included the distal Purkinje network in an anatomically realistic manner with a single main right bundle branch (RBB) with one part going to the free septal wall and the other to the papillary muscle and the left bundle branch (LBB) consisting of several interconnected bundles that ramify into a complex branching network.

Spatial resolution of the His–Purkinje models was mainly determined by the resolution of the ventricular models in which they were incorporated. It varied from several millimetres (Abboud et al., 1991; Adam, 1991) to around 1 mm (Aoki et al., 1986, 1987; Wei et al., 1987, 1990; Okazaki et al., 1998; Lorange and Gulrajani, 1993; Lorange et al., 1993; Xu et al., 1996; Dube et al., 1996; Berenfeld and Abboud, 1996; Berenfeld and Jalife, 1998; Siregar et al., 1998) to 0.5 mm (Simelius et al., 2001). The models also differ in the description of cellular excitable behaviour. Some models only described the action potential (AP) depolarization phase (Pollard and Barr, 1990, 1991), a lot of the models used a rule based cellular automata approach to describe AP dynamics (Aoki et al., 1986, 1987; Wei et al., 1987, 1990; Okazaki et al., 1998; Abboud et al., 1991; Siregar et al., 1998; Simelius et al., 2001), whereas some other models used low dimensional FitzHugh–Nagumo type dynamics to describe excitable behaviour (Berenfeld and Abboud, 1996; Berenfeld and Jalife, 1998).

The reviewed models were most often used to reproduce ECGs resulting from normal and pathological excitation sequences. However, if one would like not only to reproduce ECG signals, but also study the (sub)cellular mechanisms of arrhythmias involving the His–Purkinje system, one needs to link detailed electrophysiological processes such as ischemia, ion channel mutations, ionic remodelling, early and delayed afterdepolarizations etc., to excitation propagation patterns. This requires the use of electrophysiologically detailed, species specific second generation ionic models.

In this article we present a model of the human ventricles, which includes a His–Purkinje system, is anatomically detailed, contains fibre direction anisotropy, has a good spatial resolution, and in which cell behaviour is governed by an electrophysiologically detailed model for human ventricular cells (Ten Tusscher et al., 2004; Ten Tusscher and Panfilov, 2006), with some adaptations to describe Purkinje cell behaviour (see next sections).

3. Existing Purkinje cell models

Purkinje cells are electrophysiologically different from ventricular muscle cells (Tseng and Boyden, 1989; Cordeiro et al., 1998; Yu et al., 1995; Han et al., 2002a, b). Typically, in Purkinje cells AP upstroke velocity is larger, AP plateau is lower, AP duration (APD) is longer and APD rate dependence is stronger (Balati et al., 1998; Burashnikov and Antzelevitch, 1999; Schram et al., 2002; Lu et al., 2005). In addition, when Purkinje cells are not paced they display diastolic depolarization leading to low frequency automaticity (Yu et al., 1995; Balati et al., 1998), allowing them to function as a backup pacemaker, a property that is absent from healthy ventricular cells. Finally, Purkinje cells have no T tubules and, as a consequence, have substantially different intracellular calcium dynamics (Cordeiro et al., 2001a, b). Purkinje cells are for example much more prone to early and delayed afterdepolarizations (Cordeiro et al., 2001a).

The first cardiac electrophysiological model to be developed was the Noble (1962) model for Purkinje fibres. It was inspired on the Hodgkin–Huxley model for squid nerve action potentials and modified to reproduce the long plateau duration of cardiac APs. The model only contained a sodium current, a potassium current and a leakage current. As the slow inward calcium current had not been discovered then, the sodium was responsible for both the upstroke and plateau phase of the AP.

McAllister et al. (1975) subsequently developed an improved description for Purkinje fibre AP dynamics, based largely on detailed experimental data from sheep Purkinje fibre preparations. This model incorporated a slow inward calcium current responsible for the AP plateau. In addition, the description of potassium currents was further refined. Deactivation of the I_{K2} potassium current was mainly responsible for the development of the pacemaker potential leading to automaticity. The model contained no specific pacemaker currents, these were described and included at a later stage (see for example, DiFrancesco, 1984).

In 1985, DiFrancesco and Noble (1985) developed a further improvement of the Purkinje cell model, in which pump and exchanger currents, concentration changes and a specific pacemaker current were modelled.

To our best knowledge, this is the most recent available Purkinje cell model. The DiFrancesco–Noble model and its predecessors were largely based on experimental data from sheep Purkinje fibres.

Experimental studies have shown that Purkinje cell electrophysiological properties are species dependent (see for example, Lu et al., 2001). Therefore, the development of an anatomical His–Purkinje model for a particular species will require the development of a Purkinje cell model for that species. A detailed model for Purkinje cells should incorporate all known differences relative to ventricular muscle cells in terms of size, dynamics and presence of ionic currents (Tseng and Boyden, 1989; Cordeiro et al., 1998; Yu et al., 1995; Han et al., 2002a, b; Schram et al., 2002), plateau potentials and AP restitution (Balati et al., 1998; Burashnikov and Antzelevitch, 1999; Lu et al., 2005), and calcium handling (Cordeiro et al., 2001a, b), and should include pacemaker potentials and automaticity (Yu et al., 1995; Balati et al., 1998). Unfortunately, in recent years the attention for electrophysiologically detailed species specific modelling of cardiac cells has been aimed mainly at atrial and ventricular cells (Courtemanche et al., 1998; Nygren et al., 1998; Priebe and Beuckelmann, 1998; Iyer et al., 2004; Ten Tusscher et al., 2004; Ten Tusscher and Panfilov, 2006), and no model for human Purkinje cells has been developed.

4. Methods

4.1. Electrophysiological model

By neglecting the discrete character of microscopic cardiac cell structure, the excitable behaviour of cardiac tissue can be modelled as a continuous system using the following partial differential equation (Keener and Sneyd, 1998), usually referred to as the monodomain model:

$$C_m \frac{\partial V_m}{\partial t} = \frac{\partial}{\partial x_i} D_{ij} \frac{\partial}{\partial x_j} V_m - I_{\text{ion}}, \quad (1)$$

where C_m denotes the cellular capacitance, and I_{ion} is the sum of the ionic transmembrane currents that together generate the AP. D_{ij} is a 3D tensor describing muscle conductivity anisotropy and can be found as the ratio of the conductivity tensor and the surface to volume ratio (Qu et al., 1999). D_{ij} is determined by the local muscle fibre direction field (see next section).

To represent the electrophysiological properties specific for human ventricular tissue, we use a detailed ionic model for human ventricular myocytes that describes the dynamics of the individual ionic currents, and that is based on a large range of human electrophysiological data (Ten Tusscher et al., 2004; Ten Tusscher and Panfilov, 2006). For Purkinje cells, we use a modification of this model in which we incorporate the electrophysiological differences between Purkinje and ventricular muscle cells that are considered most important for our current purposes: the longer APD and higher AP upstroke velocity of Purkinje cells.

Longer APD is achieved by using a lower conductance for the slow delayed rectifier current ($G_{K_s, \text{purkinje}} = 0.35 G_{K_s, \text{muscle}}$) (consistent with lower I_{K_s} as suggested from lower mRNA levels, Han et al., 2002a). A higher upstroke velocity is obtained by using a higher conductance for the fast sodium current ($G_{Na, \text{purkinje}} = 2.94 G_{Na, \text{muscle}}$) (consistent with a larger effect of TTX induced I_{Na} block in Purkinje cells, than in ventricular cells, Balati et al., 1998). For simplicity, we assumed cell properties within the Purkinje system and within the ventricular mass to be homogeneous.

Fig. 2 shows APs for single ventricular and Purkinje cells in our model at 1 Hz pacing. We can see that simulated Purkinje APD is 80 ms longer than ventricular APD (387 ms versus 307 ms). Upstroke velocity is 519 V/s in Purkinje cells, versus 291 V/s in muscle cells, consistent with findings of Schram et al. (2002).

4.2. Human ventricular anatomy and anisotropy

A description of the geometry of the human ventricular myocardium was derived from anatomical data from an excised, structurally normal heart (Hren, 1996). Briefly, the heart was positioned as in the thorax and sectioned in 1 mm slices. Boundary lines of the ventricular myocardium were carefully determined in each section. These boundary line data were then digitized, and the data for the individual slices were stacked on top of one another in a 3D coordinate system, with the z-axis coinciding with the ventricular long axis.

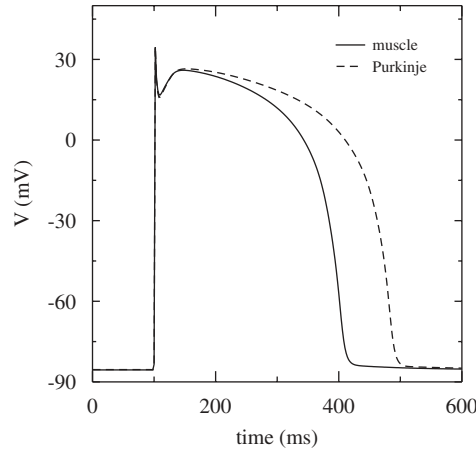


Fig. 2. Steady state APD at 1 Hz pacing for ventricular muscle and Purkinje cells for the default parameter setting of our human ventricular cell model (see Table 1 in Ten Tusscher and Panfilov, 2006). $G_{Ks, purkinje} = 0.35G_{Ks, muscle}$, $G_{Na, purkinje} = 2.94G_{Na, muscle}$.

The space was filled with a cubic lattice ($\Delta x = 0.5$ mm) and the resulting structure represented the geometry of a ventricular myocardium with nearly 1.7 million voxels (each with $\Delta V = 0.125$ mm³).

AP propagation occurs faster in the direction parallel to the muscle fibres, than in the direction perpendicular to the muscle fibres. To take the influence of muscle fibre direction on AP propagation into account, we need a detailed description of the ventricular myocardial fibre direction field. This description was originally derived from detailed data on the fibre architecture in the canine heart (Nielson et al., 1991), together with the at that time available data on human fibre architecture (Streeter, 1979). We validated this fibre direction description against more detailed recent data from human ventricles (Winslow, 2004).

The fibre direction field is used to derive the local conductivity tensor D_{ij} from the local fibre direction vector α . Assuming that transverse conductivity is the same in all directions orthogonal to the direction of the muscle fibre axis, we described the ventricular conductivity tensor using the following equation:

$$D_{ij} = D_L * \delta_{ij} + (D_L - D_T)\alpha_i\alpha_j, \quad (2)$$

where α is the vector describing the local muscle fibre direction and D_L and D_T are the conductivities in the longitudinal and transverse fibre directions, respectively. For D_L we use $162 \Omega \text{cm}$, which results in a longitudinal conduction velocity of approximately 70 cm/s, in agreement with experimentally reported values in human ventricular tissue (Taggart et al., 2000). We use a value of 2:1 for conduction velocity anisotropy, based on experimentally recorded ratios (Taggart et al., 2000) and hence a ratio of 4:1 for $D_L : D_T$.

To achieve experimentally observed maximum conduction velocities in the Purkinje system of around 3 m/s (Bigger and Mandel, 1970; Kassebaum and Van Dyke, 1966), we use a 3-fold increased I_{Na} conductance (see previous section) and a 8-fold higher conductance in the Purkinje tissue than in the ventricular tissue (in the longitudinal direction). PMJs are modelled as a connection of two regions with different conductivities (Purkinje system and ventricular muscle mass) and local Laplacians are adjusted accordingly.

4.3. Numerical integration

We use a forward Euler scheme to integrate Eq. (1), using a time step of $\Delta t = 0.02$ ms and a space step of $\Delta x = 0.5$ mm. To integrate Eq. (1), we need to evaluate at each point of the ventricular geometry the following Laplacian:

$$L(I, J, K) = \frac{\partial}{\partial x_i} D_{ij} \frac{\partial}{\partial x_j} V_m. \quad (3)$$

This Laplacian can be discretized to the following equation:

$$L(I, J, K) = \sum_{l=0}^{18} w_l V_m(l), \quad (4)$$

where l is an index running over the 18 neighbours of the point (I, J, K) and the point itself, and w_l is the weight with which the voltage of a particular neighbour grid point contributes to the Laplacian of the point (I, J, K) . The weights w_l are computed based on the local conductivity tensor and the local boundary situation in the point (I, J, K) : a neighbour l that lies outside the heart geometry receives a weight $w_l = 0$. The weights are precomputed and stored as an efficient means to evaluate the Laplacian and automatically handle boundary conditions during the simulations. The exact procedure for finding weights can be found in the article by Clayton and Panfilov in this issue.

Purkinje fibres are only electrically connected to the ventricular mass at designated positions called PMJs. At all other positions Purkinje cells are isolated from the ventricular mass via connective tissue sheets. To take this into account in our model, at non-PMJ sites, a Purkinje cell with a neighbour l being a ventricular muscle cell receives a weight $w_l = 0$, similarly a muscle cell with a neighbour l being a Purkinje cell also receives a weight $w_l = 0$.

4.4. Implementation

All simulations were coded in C++ and MPI and were run on 20 processors of a Beowulf cluster consisting of 10 Dell 650 Precision Workstations (dual Intel xeon 2.66 GHz). With this approach, simulating 1 s of wave propagation in the ventricles took about 12 h of computational time. For visualization we used the marching cubes algorithm for isosurface detection in voxel data and OpenGL for isosurface rendering.

4.5. Development of the His–Purkinje conduction system

The RBB usually originates from the most distal part of the His bundle as a single slender bundle and crosses through the muscular interventricular septum to the right ventricular (RV) endocardial septal wall (James and Sherf, 1971; Massing and James, 1976). The bundle emerges at the right septal surface and continues to the moderator band, where it branches into two different parts, one carrying excitation to the anterior papillary muscle, and the other to the RV free wall (Keith and Flack, 1906).

The LBB has a highly variable anatomy in different individuals (Massing and James, 1976). Generally speaking, the LBB consists of three main branches with multiple interconnections, which ramify over the left ventricular (LV) septal wall and extend to the bases of the anterior and posterior papillary muscles, carrying excitation to the septum and the inferior and superior free wall (Keith and Flack, 1906; Spach et al., 1963; Massing and James, 1976). No conduction network has been found in the posterior free wall of the left ventricle.

To incorporate a His–Purkinje system in our human ventricular anatomy, we followed an approach similar to the one taken by Simelius et al. (2001). We developed interactive graphical software allowing us to design the position of Purkinje–muscle insertion sites or junctions (PMJs) and of Purkinje cables on top of the endocardial surfaces of the left and right ventricles. The initial position of insertion sites and cables was based on the above described anatomical knowledge and the known sites of earliest endocardial activation reported by Durrer et al. (1970). Subsequently, the position of insertion sites, cables, cable lengths, cable thickness and conductivities were iteratively adjusted to arrive at a correct and numerically stable normal activation sequence. In the final version of our Purkinje system model we used a conductivity that is 8 times larger than in the ventricular muscle mass, together with a fast sodium current conductance that is 3 times higher than in the ventricles. The average radius of Purkinje cables was 2–3 grid points. Together this resulted in fast and stable propagation in the Purkinje system and across PMJs. Note that the Purkinje cable radius does not reflect the anatomical thickness of Purkinje fibres.

Figs. 3A and B show the developed Purkinje system on the RV septum and the RV free wall. Purkinje fibres are drawn in blue, PMJ sites in green, and the endocardial surface is drawn in red. We can see that the right

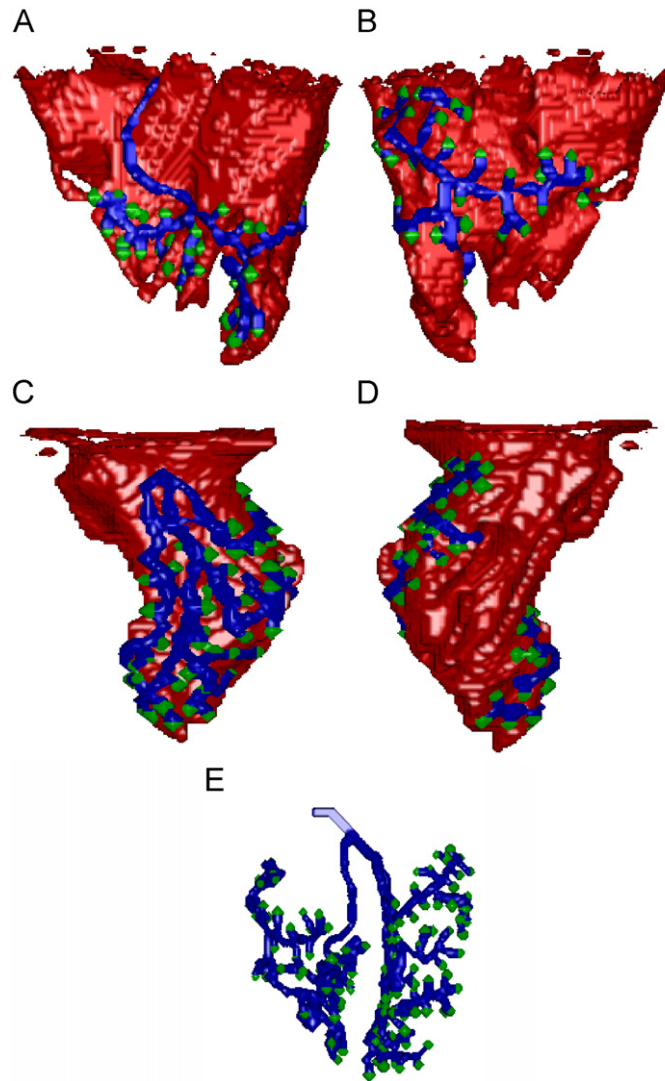


Fig. 3. (A) Septal view of the right ventricular Purkinje system. (B) Right Purkinje system on the free wall of the right ventricle. (C) Septal view of the left ventricular Purkinje system. (D) Left Purkinje system on the free wall of the left ventricle. (E) Front view of the complete His–Purkinje system, with the common His bundle and the left and right Tawara branches connecting the left and right Purkinje systems.

Purkinje system starts as a single main branch on the right septal surface, before splitting into two parts: one part ramifying on the right septum and papillary muscle and the other part ramifying on the right lateral free wall. In total, we modelled 54 PMJs in the RV Purkinje system.

Figs. 3C and D show the Purkinje system on the LV septum and the LV free wall. We can see the presence of three main interconnected branches on the left septal wall that ramify into a network on the lower left septal wall that contains numerous insertion sites. We also see the absence of insertion sites in a spiral shaped area on the LV free wall, consistent with the later activation observed in these areas by Durrer et al. (1970). In total, we modelled 76 PMJs in the LV Purkinje system. Together with the RV PMJs this results in a total of 130 PMJs in our Purkinje model.

Fig. 3E shows our complete His–Purkinje system model, with the left and right Purkinje systems connected via the left and right Tawara branches and common His bundle. The system consists of 22 426 grid points, with 20 891 grid points being Purkinje cable cells and 1535 grid points functioning as Purkinje insertion cells.

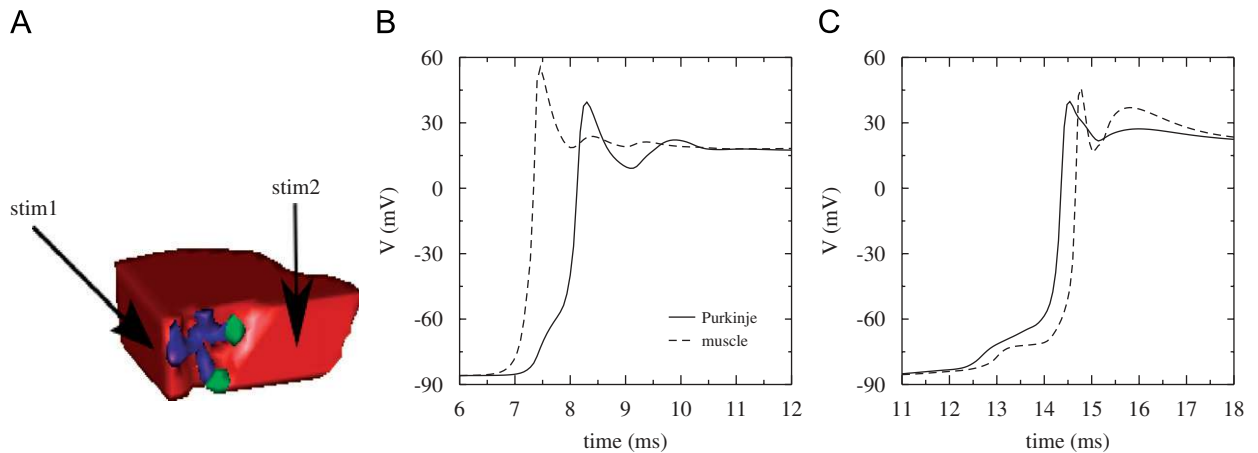


Fig. 4. Asymmetrical anterograde and retrograde conduction across the Purkinje–muscle junction. (A) Small part of the free wall of the left ventricle with short length of Purkinje cable and two PMJs. In the first stimulation protocol (stim1) the begin of the Purkinje cable is stimulated, resulting in Purkinje to muscle conduction. In the second stimulation protocol (stim2) a point in the muscle mass is stimulated, resulting in muscle to Purkinje conduction. (B) Initial phases of action potentials in a Purkinje insertion cell of the upper PMJ and a nearby muscle cell when propagation proceeds from Purkinje to muscle. (C) Initial phases of action potentials in the same cells but when propagation proceeds from muscle to Purkinje.

Note that a single PMJ site is made up of a number of Purkinje insertion cells (on average around 12), to ensure safe anterograde propagation from the Purkinje system to the myocardium.

Note that in our model Purkinje fibres end on insertion points which lie on the endocardial surface of the ventricles. We consider this to be a fair approximation since in the human heart Purkinje fibres are known to penetrate only a small portion of the ventricular wall (Coghlan et al., 2006).

It is well known that anterograde propagation from the Purkinje system to the ventricular muscle mass occurs with a lower margin of safety and a larger delay than propagation in the opposite direction. Under normal, healthy conditions Purkinje muscle conduction delays on the order of 1–2 ms have been measured (Mendez et al., 1970). Fig. 4A shows a small part of the free wall of the left ventricle with a short length of Purkinje cable and two PMJs on the endocardial surface. We record APs in the upper PMJ and in a neighbouring ventricular muscle cell for two different stimulation protocols. In the first protocol we stimulate the beginning of the Purkinje cable, such that activation proceeds from Purkinje cable to Purkinje insertion to muscle. Fig. 4B shows the initial phase of the APs in the PMJ and muscle cell for this protocol. We see a Purkinje muscle delay of around 1 ms. In the second protocol we stimulate the muscle mass, such that activation proceeds from muscle to Purkinje insertion site to Purkinje cable. Fig. 4C shows the AP beginnings in the PMJ and muscle cell for this protocol. We see that for retrograde conduction the delay from muscle to Purkinje is significantly shorter, consistent with experimental results (Mendez et al., 1970).

5. Results

5.1. Normal activation sequence

Fig. 5 shows the normal progression of excitation in the Purkinje system and ventricles when the upper part of the His bundle is stimulated. We see that the wave (yellow) progresses from the His bundle to the left and right branches of the Purkinje system. Propagation on the left side goes somewhat faster, due to the presence of three left branches as opposed to one right main branch. At first the wave propagates only through the Purkinje system, with no muscle cells being excited. At 50 ms the wave has reached the first PMJs and starts to progress through the ventricular muscle mass. This agrees with clinically reported normal His ventricle intervals (Li et al., 2002). The excitation of the Purkinje system is complete within 90 ms, whereas excitation of the ventricles is complete after 150 ms. Activation of the ventricular mass takes 100 ms: it starts at 50 ms and finishes at 150 ms.

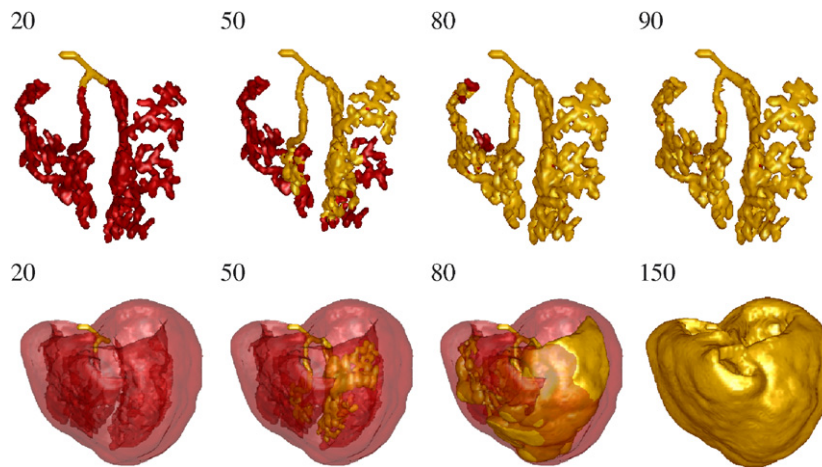


Fig. 5. Normal activation sequence. Time is counted in ms from the moment the upper part of the His bundle is stimulated. In the top row, only the propagation of the wave through the Purkinje system is displayed. In the bottom row, propagation through the Purkinje system and ventricles is displayed. Snapshots are taken at the indicated times. (Top row) Normal activation sequence in the Purkinje system. (Bottom row) Normal activation sequence in the ventricles and Purkinje system.

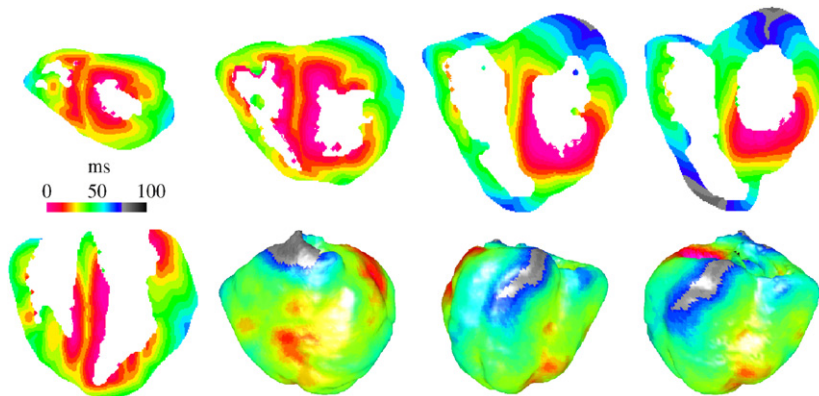


Fig. 6. Colour isochrones of the normal activation sequence. Time is counted from the moment of first endocardial activation, rather than from the moment of upper His bundle stimulation, to allow better comparison with the data from Durrer et al. (1970). (Top row) Normal activation sequence in horizontal cross-sections of the ventricles. Cross-sections were chosen to agree closely with the horizontal cross-sections shown in Fig. 1 of Durrer et al. (1970). We use a similar colour scheme as in Durrer et al. (1970). (Bottom row, left) Normal activation in a transversal section of the ventricles, similar to the section shown in Fig. 2 of the paper by Durrer et al. (1970). (Bottom row, rest) Normal activation on the anterior, left lateral and posterior epicardial surfaces, similar to those shown in Fig. 4 of Durrer et al. (1970).

Fig. 6 shows isochrones of the same normal activation sequence as in Fig. 5. The horizontal and transversal cross-sections have been chosen at similar locations as the sections shown in Figs. 1 and 2 in the paper by Durrer et al. (1970). In addition we show anterior and posterior views of the epicardial surface, similar to Fig. 4 in Durrer et al. (1970).

Our simulated activation sequence shows a good agreement with the experimental data obtained from explanted human hearts by Durrer et al. (1970). Earliest endocardial activation in the left ventricle occurs high on the anterior paraseptal wall (pictures 3 and 4 of top row), central on the left surface of the interventricular septum (pictures 1 and 2 of top row) and on the lower posterior paraseptal wall (pictures 1 and 2). As in Durrer's data, the posterobasal part of the left ventricle is the last part to activate (pictures 3 and 4 in top row, pictures 3 and 4 bottom row). Earliest endocardial activation of the right ventricle starts on the lower and central right surface of the interventricular septum (pictures 1 and 2 of top row). Total activation of the

ventricles took approximately 100 ms. This is somewhat longer than the time observed by Durrer et al. However, as was shown by Durrer et al., isolation of the heart seems to increase conduction velocity and decrease total excitation time. Furthermore, a total activation time of 100 ms is well within the range of normal healthy QRS durations.

5.2. Bundle branch block

One of the more frequently occurring abnormalities in Purkinje and ventricular activation are the so-called bundle branch blocks. Under conditions of consistent bundle branch block, one of the bundle branches fully blocks propagation of the excitation wave, whereas the other bundle branch conducts the excitation wave. As a consequence, the ventricle that is on the side of the non-conducting bundle branch will not be excited by its own Purkinje system, but will rather be excited indirectly via the other ventricle. This will lead to a delay in activation of that ventricle.

Bundle branch block may occur in patients without any apparent heart disease (Niu et al., 2006), but frequently occurs in patients with heart failure (Fantoni et al., 2005), hypertension, ischemic heart disease and LV hypertrophy (Imanishi et al., 2006).

Here we simulate bundle branch block by keeping a small region in the blocked Purkinje branch at the resting potential, prohibiting propagation of the excitation wave through this region. All other model parameters are the same as under the conditions of normal excitation.

Fig. 7, top row, shows activation in the Purkinje system and ventricles when we simulate a right bundle branch block (RBBB). We can see that propagation in the Purkinje system proceeds in the left half but is blocked in the right half of the system. We can also see that no excitation of the right ventricle occurs directly via the Purkinje system, but that instead a delayed activation occurs by a progression of the excitation wave from the LV muscle mass to the right ventricle. We can see that the activation of the left ventricle, which has a normal conducting Purkinje system, is very similar to the activation pattern under normal conditions (compare Fig. 7, bottom row, with Fig. 6). In contrast, the activation pattern of the right ventricle can be seen to be significantly delayed relative to the normal activation sequence and can be seen to progress from the left ventricle. Under these conditions, total excitation of the ventricles takes approximately 130 ms, which is 30 ms longer than under normal conditions.

Fig. 8, top row, shows excitation of the Purkinje system and ventricles during simulated left bundle branch block (LBBB). Propagation is blocked in the branch of the Purkinje system, hence excitation of the left ventricle occurs through the excitation wave in the right ventricle. Fig. 8, bottom row, shows isochrones of the activation pattern resulting from LBBB. In this case the RV activation pattern resembles the normal

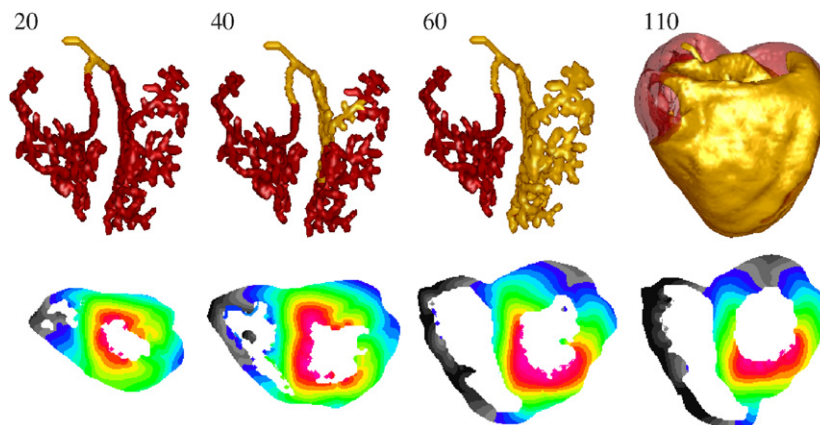


Fig. 7. (Top row, first three pictures) Activation sequence in the Purkinje system under simulated right bundle branch block. (Top row, fourth pictures) Activation in the ventricles and Purkinje system under right bundle branch block. The left ventricle is excited directly via its Purkinje system. The right ventricle is excited indirectly via the left ventricle. (Bottom row) Colour isochrones of right bundle branch block activation in horizontal layers of the ventricles. Colour scheme the same as in Fig. 5.

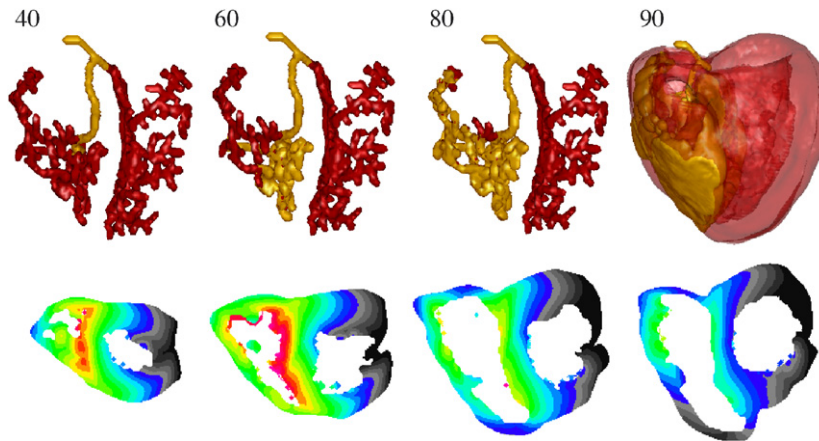


Fig. 8. (Top row, first three pictures) Activation sequence in the Purkinje system under simulated left bundle branch block. (Top row, fourth pictures) Activation in the ventricles and Purkinje system under left bundle branch block. The right ventricle is excited directly via its Purkinje system. The left ventricle is excited indirectly via the right ventricle. (Bottom row) Colour isochrones of left bundle branch block activation in horizontal layers of the ventricles. Colour scheme the same as in Fig. 5.

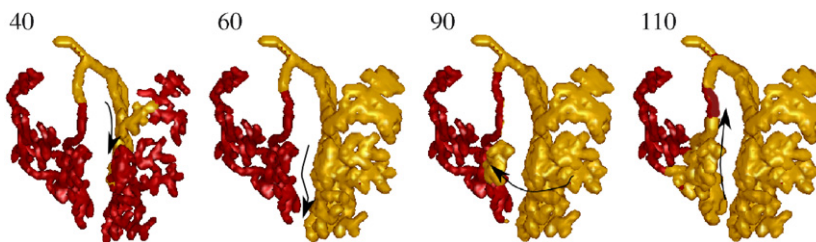


Fig. 9. Failed attempt to simulate right bundle branch reentry. Activation sequence in the Purkinje system under simulated temporal conduction block in the right Purkinje branch. Arrows indicate the direction of wave propagation. Excitation goes from the left bundle branch to the septum, up the right bundle branch, toward the left bundle branch where it runs into the previous excitation wave. The effective circuit length is too short to induce sustained reentry.

activation pattern, whereas the LV activation is severely delayed and originates from the right ventricle. Full excitation of the ventricles now takes 140 ms, which is 40 ms longer than under normal conditions.

The elongation of 30–40 ms observed in our model for right and left bundle branch block, respectively, is consistent with the elongated QRS durations of ~140–150 and ~150–160 ms associated with right and left bundle branch patterns in patients (Fantoni et al., 2005; Niu et al., 2006). The larger increase in activation time caused by LBBB relative to RBBB is also consistent with clinical data (Fantoni et al., 2005; Niu et al., 2006).

5.3. Bundle branch reentry

Another anomaly occurring in Purkinje–ventricular excitation is bundle branch reentry. For bundle branch reentry to occur two conditions need to be satisfied. First, a temporary unidirectional conduction block needs to occur in one of the bundle branches. Second, the path length in the reentry circuit needs to be long enough to enable reentry of the wave. The reentry circuit consists of the non-blocking anterograde conducting Purkinje branch, part of the ventricular muscle mass, and the temporary blocking now retrograde conducting Purkinje branch. Whether the path length is long enough will depend on conduction velocities in the Purkinje system and septal muscle mass, the route the excitation wave follows along the Purkinje network and through the myocardium, and APD in the Purkinje system and muscle mass.

Fig. 9 shows an attempt at simulating bundle branch reentry by temporary blocking conduction in the right branch of the Purkinje system, while all other model settings are the same as in the normal and bundle branch settings. We can see that retrograde activation of insertion points in the right Purkinje system occurs and leads to retrograde wave propagation up the Purkinje network. However, when the excitation wave arrives at the top of the right Purkinje network, it cannot proceed to excite the left Purkinje network, as this is still refractory. This implies that under normal conditions, even in the presence of a temporary block in one of the bundle branches, no sustained bundle branch reentry can occur.

Bundle branch reentry underlies an estimated 6–7% of sustained ventricular tachycardias of non-ischemic origin. Cardiac diseases associated with bundle branch reentry are different forms of cardiomyopathy, congestive heart failure, atherosclerosis, previous infarction and aortic valve regurgitation (Caceres et al., 1989). In patients with bundle branch reentry cardiac enlargement, delays in the Purkinje ventricular conduction time and interventricular conduction delays are reported (Caceres et al., 1989; Merino et al., 1998; Li et al., 2002; Mazur et al., 2005).

We were able to reproduce bundle branch reentry in our model: however, in order to achieve this we needed to increase the effective path length for reentry in our heart model by decreasing conductivity of the Purkinje system and decreasing sodium current conductance in both the Purkinje system and ventricles. During normal sinus rhythm, this modification resulted in a His ventricle interval of 100 ms, 50 ms longer than the normal interval of 50 ms, consistent with the prolonged His ventricle intervals found in most patients with bundle branch reentry (Caceres et al., 1989; Merino et al., 1998; Li et al., 2002).

Fig. 10 shows an example of sustained bundle branch reentry. Temporary unidirectional block occurred in the RBB, leading to a reentry circuit with anterograde propagation in the left and retrograde propagation in the RBB. Excitation crosses from the left to the right bundle branches via excitation of PMJs on the left side of the septum, leading to septal activation in a left to right manner, and excitation of PMJs on the right side of the septum. Excitation thus crosses from left to right before the entire left Purkinje system has become excited. Fig. 11 schematically shows the reentry circuit followed. The simulated sustained bundle branch reentry results in an excitation frequency of 3.2 Hz, consistent with clinically observed frequencies of 2.8–4 Hz in patients

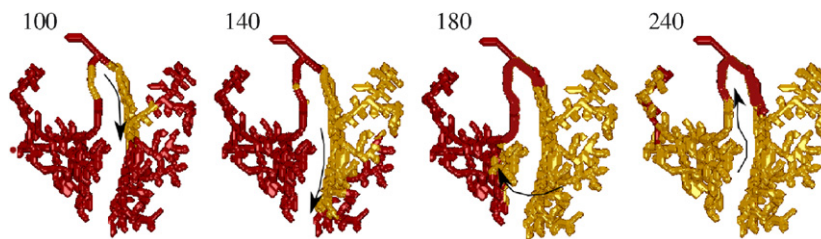


Fig. 10. Successful attempt to simulate right bundle branch reentry. In order to get sustained bundle branch reentry, the effective path length of the reentry circuit needs to be increased. We achieved this by lowering conductance in the Purkinje system ($D_{\text{pur,BBreentry}} = 0.125 * D_{\text{pur,normal}}$) and by lowering sodium current in both the ventricles and Purkinje system ($I_{\text{Na,BBreentry}} = 0.4I_{\text{Na,normal}}$).



Fig. 11. Schematic indication of the reentry path followed by the sustained reentry of Fig. 10.

with sustained bundle branch reentry ventricular tachycardia (Caceres et al., 1989; Mazur et al., 2005). We found similar results for simulating a temporal unidirectional block in the LBB (data not shown).

Note that although His–ventricle delays and reentry frequencies in our models are consistent with clinical results, our model currently only reproduces the effective path length and rotation time of bundle branch reentry rather than the detailed cellular, tissue and heart size abnormalities that lead to bundle branch reentry.

6. Discussion

The Purkinje system plays an important role in normal and abnormal excitation of the ventricles. To investigate the precise role of the Purkinje system in these processes using a modelling approach, a model of the Purkinje system needs to be incorporated in our human ventricles model.

In this paper we review previously developed His–Purkinje–ventricles models and describe the development and incorporation of a His–Purkinje system in our human ventricles model. Our model is based on anatomical data and on experimental data of the normal activation sequence of the human heart. We designed our model using an interactive graphical program and iteratively adjusted topology, cable thickness and conductivity of the Purkinje network and Purkinje–muscle insertion sites to achieve a good agreement with the activation sequence generated by our model and the known normal human cardiac activation sequence.

We show that our His–Purkinje–ventricles model indeed generates a normal activation sequence that closely resembles the activation sequence data recorded by Durrer et al. (1970). In addition, we use our model to simulate activation sequences resulting from left or right bundle branch block. We demonstrate delayed activation of the left or right ventricle, and longer total ventricular activation time, consistent with clinical findings (Fantoni et al., 2005; Niu et al., 2006).

Finally, we use our His–Purkinje–ventricles model to investigate the phenomenon of sustained bundle branch reentry. We show that under normal conditions, sustained reentry cannot occur since the effective path length will be too short. We demonstrate that under conditions of hampered conductance in both the Purkinje network and the ventricular mass effective path length can be increased such that sustained reentry can occur. This agrees with the fact that bundle branch reentry driven sustained tachycardia occurs in patients with delays in Purkinje ventricle activation times and interventricular conductance (Caceres et al., 1989; Mazur et al., 2005).

Apart from playing a role in bundle branch block and bundle branch reentry, the Purkinje system may play a role in more complex arrhythmias. During ventricular tachycardia and fibrillation, often focal subendocardial activations are observed (Pogwizd and Corr, 1992; Chung et al., 1997; Pogwizd et al., 1998; Arnar et al., 1997, 2001; Arnar and Martins, 2002). These activations can be due to micro-reentry involving the Purkinje system, triggered activity in the Purkinje system, or abnormal automaticity of the Purkinje system. Which of these mechanisms may play a role during tachyarrhythmias remains to be investigated.

Furthermore, the presence of the Purkinje system adds heterogeneity in APD dynamics, adds alternative routes for excitation waves, and influences local source sink relationships. These factors may potentially influence initiation, maintenance, drift or stability of scroll waves present in the ventricular mass. It remains to be investigated whether and how the Purkinje system influences vulnerability to arrhythmias and arrhythmia dynamics.

6.1. Limitations

There are a number of limitations to our human His–Purkinje–ventricle models.

First, we assume that transverse conductivity is the same in all directions orthogonal to the direction of the muscle fibre axis. However, due to the fact that cardiac muscle fibres are organized into laminar tissue sheets that are separated by connective tissue, conductivity transversal to the tissue planes is less strong than conductivity transversal to the muscle fibres but in the tissue sheets (LeGrice et al., 1995; Hunter et al., 1997; Hooks et al., 2002). This may influence both normal and abnormal propagation patterns. However, given the small differences found between the two transversal conductivities in a modelling study investigating the effect of laminar sheets on wave propagation (Hooks et al., 2002), we do not expect to obtain very different excitation patterns when this orthotropic anisotropy is incorporated into our model.

A second limitation of our model is that within the ventricular mass and within the Purkinje system, cell properties are homogeneous. Real cardiac tissue is heterogeneous with respect to AP shape, duration and rate dependence. Well known heterogeneities present in the heart are, for example, the transmural epicardial–M cell–endocardial, the base–apex and the left–right ventricular gradients (Burton and Cobbe, 2001; Liu and Antzelevitch, 1995; Zygmunt et al., 2000; Samie et al., 2001). Heterogeneities in Purkinje cell properties have also been reported (Verkerk et al., 1999). These heterogeneities are expected to influence mainly the repolarization and not so much the activation phase of the cardiac cycle. As such they may be important for the correct genesis of the normal cardiac repolarization sequence and the associated T wave, but also in the precise conditions for vulnerability to wave breaks and size of reentry cycles. We plan to incorporate such heterogeneities in future versions of our model.

A third limitation of our model lies in the electrophysiological description of the Purkinje cells. Currently, to describe Purkinje cells we use a modestly modified version of our human ventricular cell model in which we take the longer AP duration and steeper upstroke phase of Purkinje cells in to account. Obviously, a more detailed human Purkinje cell model based on experimental human Purkinje cell data, and including pacemaker potential development and the substantial differences in intracellular calcium handling is needed, if we want to study, for example, the potential role of abnormal automaticity in Purkinje cells, or under what precise conditions EADs and DADs develop in Purkinje cells. Developing such a model was outside the scope of the present article.

A final limitation of our model lies in the way we modelled bundle branch reentry. Currently, the temporal bundle branch block and increase in effective path length required to get sustained bundle branch reentry are obtained in a phenomenological manner, rather than in a biophysically detailed way reflecting a particular disease state that leads to the onset and maintenance of reentry.

Acknowledgement

This work was supported by the Netherlands Organisation for Scientific Research (NWO) through Grant number 635100004 of the Research Council for Physical Sciences (EW) (K.H.W.J. Ten Tusscher).

References

- Abboud, S., Berenfeld, O., Sadeh, H., 1991. Simulation of high-resolution QRS complex using a ventricular model with a fractal conduction system. Effects of ischemia on high-frequency QRS potentials. *Circ. Res.* 68, 1751–1760.
- Adam, D.R., 1991. Propagation of depolarization and repolarization processes in the myocardium—an anisotropic model. *IEEE Trans. Biomed. Eng.* 38, 133–141.
- Aoki, M., Okamoto, Y., Musha, T., Harumi, K., 1986. 3-Dimensional computer simulation of depolarization and repolarization processes in the myocardium. *Jpn. Heart J.* 27 (S1), 225–234.
- Aoki, M., Okamoto, Y., Musha, T., Harumi, K., 1987. Three-dimensional simulation of the ventricular depolarization and repolarization processes and body surface potentials: normal heart and bundle branch block. *IEEE Trans. Biomed. Eng.* 34, 454–462.
- Arnar, D.O., Martins, J.B., 2002. Purkinje involvement in arrhythmias after coronary artery reperfusion. *Am. J. Physiol. Heart Circ. Physiol.* 282, H1189–H1196.
- Arnar, D.O., Bulling, J.R., Martins, J.B., 1997. Role of the Purkinje system in spontaneous ventricular tachycardia during acute ischemia in a canine model. *Circulation* 96, 2421–2429.
- Arnar, D.O., Xing, D., Lee, H., Martins, J.B., 2001. Prevention of ischemic ventricular tachycardia of Purkinje origin: role for alpha(2)-adrenoceptors in Purkinje? *Am. J. Physiol. Heart Circ. Physiol.* 280, H1182–H1190.
- Balati, B., Varro, A., Papp, J.G., 1998. Comparison of the cellular electrophysiological characteristics of canine left ventricular epicardium, m cells, endocardium and Purkinje fibres. *Acta Physiol. Scand.* 164, 181–190.
- Berenfeld, O., Abboud, S., 1996. Simulation of cardiac activity and the EGG using a heart model with a reaction–diffusion action potential. *Med. Eng. Phys.* 18, 615–625.
- Berenfeld, O., Jalife, J., 1998. Purkinje–muscle reentry as a mechanism of polymorphic ventricular arrhythmias in a 3-dimensional model of the ventricles. *Circ. Res.* 82, 1063–1077.
- Berne, R.M., Levy, M.N., 1993. *Physiology. The Cardiac Pump.* Mosby Year Book (Chapter 24).
- Bigger, J.T., Mandel, W.J., 1970. Effect of lidocaine on conduction in canine Purkinje fibers and at the ventricular muscle–Purkinje fiber junction. *J. Pharmacol. Exp. Ther.* 172, 239–254.
- Burashnikov, A., Antzelevitch, C., 1999. Differences in the electrophysiologic response of four canine ventricular cell types to alpha-1-adrenergic agonists. *Cardiovasc. Res.* 43, 901–908.

- Burton, F.L., Cobbe, S.M., 2001. Dispersion of ventricular repolarization and refractory period. *Cardiovasc. Res.* 50, 10–23.
- Caceres, J., Jazayeri, M., McKinnie, J., Avitall, B., Denker, S.T., Tchou, P., Akhtar, M., 1989. Sustained bundle branch reentry as a mechanism of clinical tachycardia. *Circulation* 79, 256–270.
- Chung, M.K., Pogwizd, S.M., Miller, D.P., Cain, M.E., 1997. Three-dimensional mapping of the initiation of nonsustained ventricular tachycardia in the human heart. *Circulation* 95, 2517–2527.
- Clements, C.J., Vigmond, E.J., 2005. Construction of a cardiac conduction system subject for extracellular stimulation. In: *IEEE-EMBS 2005. Proceedings of the 27th Annual International Conference of the Engineering in Medicine and Biology Society, 2005*, pp. 4235–4238.
- Coghlan, H.C., Coghlan, A.R., Buckberg, G.D., 2006. The electrical spiral of the heart: its role in the helical continuum. The hypothesis of the anisotropic conducting matrix. *Eur. J. Cardiothorac. Surg.* 295, S178–S187.
- Cordeiro, J.M., Spitzer, K.W., Giles, W.R., 1998. Repolarizing K^+ currents in rabbit heart Purkinje cells. *J. Physiol.* 508, 811–823.
- Cordeiro, J.M., Bridge, J.H.B., Spitzer, K.W., 2001a. Early and delayed afterdepolarizations in rabbit heart Purkinje cells viewed by confocal microscopy. *Cell Calcium* 29, 289–297.
- Cordeiro, J.M., Spitzer, K.W., Giles, W.R., Ershler, P.E., Cannell, M.B., Bridge, J.H.B., 2001b. Location of the initiation site of calcium transients and sparks in rabbit heart Purkinje cells. *J. Physiol.* 531, 5301–5314.
- Courtemanche, M., Ramirez, R.J., Nattel, S., 1998. Ionic mechanisms underlying human atrial action potential properties: insights from a mathematical model. *Am. J. Physiol. Heart Circ. Physiol.* 275, H301–H321.
- DiFrancesco, D., 1984. Characterization of the pace-maker current kinetics in calf Purkinje fibers. *J. Physiol.* 348, 341–367.
- DiFrancesco, D., Noble, D., 1985. A model of cardiac electrical activity incorporating ionic pumps and concentration changes. *Philos. Trans. R. Soc. London B* 307, 353–398.
- Dube, B., Gulrajani, R.M., Lorange, M., LeBlanc, A.R., Nasmith, J., Nadeau, R.A., 1996. A computer heart model incorporating anisotropic propagation. IV. Simulation of regional myocardial ischemia. *J. Electrocardiol.* 29, 91–103.
- Durrer, D., Van Dam, R.T., Freud, G.E., Janse, M.J., Meijler, F.L., Arzbacher, R.C., 1970. Total excitation of the isolated human heart. *Circulation* 41, 899–912.
- Eckert, R., Randall, D., Augustine, G., 1988. *Circulation of the Blood. Animal Physiology, Mechanisms and Adaptations*. W. H. Freeman and Company, New York (Chapter 13).
- Fantoni, C., Kawabata, M., Massaro, R., Regoli, F., Raffa, S., Arora, V., Salerno-Uriarte, J.A., Klein, H.U., Auricchio, A., 2005. Right and left ventricular activation sequence in patients with heart failure and right bundle branch block: a detailed analysis using three-dimensional non-fluoroscopic electroanatomic mapping system. *J. Cardiovasc. Electrophysiol.* 16, 112–119.
- Han, W., Bao, W., Wang, Z., Nattel, S., 2002a. Comparison of ion-channel subunit expression in canine cardiac Purkinje fibers and ventricular muscle. *Circ. Res.* 91, 790–797.
- Han, W., Zhang, L., Schram, G., Nattel, S., 2002b. Properties of potassium currents in Purkinje cells of failing human hearts. *Am. J. Physiol. Heart Circ. Physiol.* 283, H2495–H2503.
- Hooks, D.A., Tomlinson, K.A., Marsden, S.G., LeGrice, I.J., Smaill, B.H., Pullan, A.J., Hunter, P., 2002. Cardiac microstructure: implications for electrical propagation and defibrillation in the heart. *Circ. Res.* 23, 331–338.
- Hren, R., 1996. A realistic model of the human ventricular myocardium: application to the study of ectopic activation. Ph.D. Thesis, Dalhousie University, Halifax.
- Hunter, P.J., Smail, B.H., Nielson, P.M.F., LeGrice, I.J., 1997. A mathematical model of cardiac anatomy. In: Panfilov, A.V., Holden, A.V. (Eds.), *Computational Biology of the Heart*. Wiley, Chichester, pp. 171–215.
- Imanishi, R., Seta, S., Ichimaru, S., Nakashima, E., Yano, K., Akahoshi, M., 2006. Prognostic significance of incident complete left bundle branch block observed over a 40-year period. *Am. J. Cardiol.* 98, 644–648.
- Iyer, V., Mazhari, R., Winslow, R., 2004. A computational model of the human left-ventricular epicardial myocyte. *Biophys. J.* 87, 1507–1525.
- James, T.N., Sherf, L., 1971. Fine structure of the his bundle. *Circulation* 44, 9–28.
- James, T.N., Sherf, L., Urthaler, F., 1974. Fine structure of the bundle branches. *Br. Heart J.* 36, 1–18.
- Kassebaum, D.G., Van Dyke, A.R., 1966. Electrophysiological effects of isoproterenol on Purkinje fibers of the heart. *Circ. Res.* 19, 940–946.
- Keener, J., Sneyd, J., 1998. *Mathematical Physiology*. Springer, New York, Heidelberg, Berlin.
- Keith, A., Flack, M.W., 1906. The auriculo-ventricular bundle of the human heart. *Lancet* 168, 359–364.
- LeGrice, I.J., Smaill, B.H., Chai, L.Z., Edgar, S.G., Gavin, J.B., Hunter, P.J., 1995. Laminar structure of the heart: ventricular myocyte arrangement and connective tissue architecture in the dog. *Am. J. Physiol. Heart Circ. Physiol.* 269, H571–H582.
- Li, Y., Gronefeld, G., Israel, C., Bogun, F., Hohnloser, S.H., 2002. Bundle branch reentrant tachycardia in patients with apparent normal His–Purkinje conduction: the role of functional conduction impairment. *J. Cardiovasc. Electrophysiol.* 13, 1233–1239.
- Liu, D.W., Antzelevitch, C., 1995. Characteristics of the delayed rectifier current (I_{Kr} and I_{Ks}) in canine ventricular epicardial, midmyocardial, and endocardial myocytes. A weaker I_{Ks} contributes to the longer action potential of the M cell. *Circ. Res.* 76, 351–365.
- Lorange, M., Gulrajani, R.M., 1993. A computer heart model incorporating anisotropic propagation. I. Model construction and simulation of normal activation. *J. Electrocardiol.* 26, 245–261.
- Lorange, M., Gulrajani, R.M., Nadeau, R.A., Preda, I., 1993. A computer heart model incorporating anisotropic propagation. II. Simulations of conduction block. *J. Electrocardiol.* 26, 263–277.
- Lu, H.R., Marien, R., Saels, A., De Clerck, F., 2001. Species plays an important role in drug-induced prolongation of action potential duration and early afterdepolarizations in isolated Purkinje fibers. *J. Cardiovasc. Electrophysiol.* 12, 93–102.

- Lu, H.R., Vlamincx, E., Van de Water, A., Gallacher, D.J., 2005. Both beta-adrenergic receptor stimulation and cardiac tissue type have important roles in elucidating the functional effects of $i(\text{ks})$ channel blockers in vitro. *J. Pharmacol. Toxicol. Methods* 51, 81–90.
- Massing, G.K., James, T.N., 1976. Anatomical configuration of the His bundle and bundle branches in the human heart. *Circulation* 53, 609–621.
- Mazur, A., Kusniek, J., Strasberg, B., 2005. Bundle branch reentrant ventricular tachycardia. *Indian Pacing Electrophysiol. J.* 5, 86–95.
- McAllister, R.E., Noble, D., Tsien, R.W., 1975. Reconstruction of the electrical activity of cardiac Purkinje fibres. *J. Physiol.* 251, 1–59.
- Mendez, C., Mueller, W.J., Uguiaga, X., 1970. Propagation of impulses across the Purkinje fiber–muscle junctions in the dog heart. *Circ. Res.* 26, 135–150.
- Merino, J., Carmona, J., Fernandez-Lozano, I., Peinado, R., Basterra, N., Sobrino, J.A., 1998. Mechanisms of sustained ventricular tachycardia in myotonic dystrophy: implications for catheter ablation. *Circulation* 98, 541–546.
- Miller, W.T., Geselowitz, D.B., 1978a. Simulation studies of the electrocardiogram. I. The normal heart. *Circ. Res.* 43, 301–315.
- Miller, W.T., Geselowitz, D.B., 1978b. Simulation studies of the electrocardiogram. II. Ischemia and infarction. *Circ. Res.* 43, 315–323.
- Nielson, P.M.F., LeGrice, I.J., Smail, B.H., Hunter, P.J., 1991. A mathematical model of the geometry and fibrous structure of the heart. *Am. J. Physiol. Heart Circ. Physiol.* 260, H1365–H1378.
- Niu, H.X., Hua, W., Zhang, S., Sun, X., Wang, F.Z., Chen, K.P., Wang, H., Chen, X., 2006. Assessment of cardiac function and synchronicity in subjects with isolated bundle branch block using Doppler imaging. *Chin. Med. J.* 119, 795–800.
- Noble, D., 1962. A modification of the Hodgkin–Huxley equations applicable to Purkinje fibres action and pacemaker potential. *J. Physiol. (London)* 160, 317–352.
- Nygren, A., Fiset, C., Firek, L., Clark, J.W., Lindblad, D.S., Clark, R.B., Giles, W.R., 1998. Mathematical model of an adult human atrial cell. The role of K^+ currents in repolarization. *Circ. Res.* 82, 63–81.
- Okazaki, O., Yamauchi, Y., Kashida, M., Izumo, K., Akatsuka, N., Ohnishi, S., Shoda, M., Nirei, H., Ebato, M., Mashima, S., Harumi, K., Wei, D., 1998. Possible mechanism of ECG features in patients with idiopathic ventricular fibrillation studied by heart model and computer simulation. *J. Electrocardiol.* 30 (S), 98–104.
- Pogwizd, S.M., Corr, B., 1992. The contribution of nonreentrant mechanisms to malignant ventricular arrhythmias. *Basic Res. Cardiol.* 87 (S2), 115–129.
- Pogwizd, S.M., McKenzie, J.P., Cain, M.E., 1998. Mechanisms underlying spontaneous and induced ventricular arrhythmias in patients with idiopathic dilated cardiomyopathy. *Circulation* 98, 2404–2414.
- Pollard, A.E., Barr, R.C., 1990. The construction of an anatomically based model of the human ventricular conduction system. *IEEE Trans. Biomed. Eng.* 37, 1173–1185.
- Pollard, A.E., Barr, R.C., 1991. Computer simulations of activation in an anatomically based model of the human ventricular conduction system. *IEEE Trans. Biomed. Eng.* 38, 982–996.
- Priebe, L., Beuckelmann, D.J., 1998. Simulation study of cellular electric properties in heart failure. *Circ. Res.* 82, 1206–1223.
- Qu, Z., Weiss, J.N., Garfinkel, A., 1999. Cardiac electrical restitution properties and stability of reentrant spiral waves: a simulation study. *Am. J. Physiol. Heart Circ. Physiol.* 276, H269–H283.
- Samie, F.H., Berenfeld, O., Anumonwo, J., Mironov, S.F., Udassi, S., Beaumont, J., Taffet, S., Pertsov, A.M., Jalife, J., 2001. Rectification of the background potassium current: a determinant of rotor dynamics in ventricular fibrillation. *Circ. Res.* 89, 1216–1223.
- Schram, G., Pourrier, M., Melnyk, P., Nattel, S., 2002. Differential distribution of cardiac ion channel expression as a basis for regional specialization in electrical function. *Circ. Res.* 90, 939–950.
- Silverman, M.E., Grove, D., Upshaw, C.B., 2006. Why does the heart beat? The discovery of the electrical system of the heart. *Circulation* 113, 2775–2781.
- Simelius, K., Nenonen, J., Horacek, M., 2001. Modeling cardiac ventricular activation. *Int. J. Bioelectromagn.* 3, 51–58.
- Siregar, P., Sinteff, J.P., Julen, N., Le Beux, P., 1998. An interactive 3d anisotropic cellular automata model of the heart. *Comput. Biomed. Res.* 31, 323–347.
- Spach, M.S., Huang, S., Armstrong, S.I., Canent, R.V., 1963. Demonstration of peripheral conduction system in human hearts. *Circulation* 28, 333–338.
- Streeter, D.D.J., 1979. Gross morphology and fiber geometry of the heart. In: *Handbook of Physiology—Section 2: The Cardiovascular System, Volume I: The Heart*. American Physiological Society, Bethesda, MD, pp. 61–112.
- Taggart, P., Sutton, P.M.I., Opthof, T., Coronel, R., Trimlett, R., Pugsley, W., Kallis, P., 2000. Inhomogeneous transmural conduction during early ischemia in patients with coronary artery disease. *J. Mol. Cell. Cardiol.* 32, 621–639.
- Tawara, S., 2000. *The Conduction System of the Mammalian Heart* (Suma, K., Shimada M., trans.). Imperial College Press, London, UK.
- Ten Tusscher, K.H.W.J., Panfilov, A.V., 2006. Alternans and spiral breakup in a human ventricular tissue model. *Am. J. Physiol. Heart Circ. Physiol.* 291, H1088–H1100.
- Ten Tusscher, K.H.W.J., Noble, D., Noble, P.J., Panfilov, A.V., 2004. A model for human ventricular tissue. *Am. J. Physiol. Heart Circ. Physiol.* 286, H1573–H1589.
- Tseng, G.N., Boyden, P.A., 1989. Multiple types of Ca^{2+} currents in single canine Purkinje cells. *Circ. Res.* 65, 1735–1750.
- Verkerk, A., Veldkamp, M.W., Abbate, F., Antoons, G., Bouman, L.N., Ravestloot, J.H., van Ginneken, A.C., 1999. Two types of action potential configuration in single cardiac Purkinje cells of sheep. *Am. J. Physiol. Heart Circ. Physiol.* 277, H1299–H1310.
- Vigmond, E.J., Clements, C.J., 2007. Construction of a computer model to investigate sawtooth effects in the Purkinje system. *IEEE TBME* 54, 389–399.
- Wei, D., Okazaki, O., Harumi, K., 1995. Comparative simulation of excitation and body surface electrocardiogram with isotropic and anisotropic computer heart models. *IEEE Trans. Biomed. Eng.* 42, 343–357.

- Wei, D.M., Aoki, M., Okamoto, Y., Musha, T., Harumi, K., 1987. Computer simulation of the Wolff–Parkinson–White syndrome utilizing a human heart model. *Jpn. Heart J.* 28, 707–718.
- Wei, D.M., Yamada, G., Musha, T., Tsunakawa, H., Tsutsumi, T., Harumi, K., 1990. Computer simulation of supraventricular tachycardia with the Wolff–Parkinson–White syndrome using three-dimensional heart models. *J. Electrocardiol.* 23, 261–273.
- Winslow, 2004. (<http://www.ccbm.jhu.edu/research/dtmrids.php>).
- Xing, D., Martins, J.B., 2004. Triggered activity due to delayed afterdepolarizations in sites of focal origin of ischemic ventricular tachycardia. *Am. J. Physiol. Heart Circ. Physiol.* 287, H2078–H2084.
- Xu, Z., Guljarani, R.M., Molin, F., Lorange, M., Dube, B., Savard, P., Nadeau, R.A., 1996. A computer heart model incorporating anisotropic propagation. III. Simulation of ectopic beats. *J. Electrocardiol.* 29, 73–90.
- Yu, H., Chang, F., Cohen, I.S., 1995. Pacemaker current I_f in adult canine cardiac ventricular myocytes. *J. Physiol.* 485, 469–483.
- Zygmunt, A.C., Goodrow, R.J., Antzelevitch, C., 2000. I_{NaCa} contributes to electrical heterogeneity within the canine ventricle. *Am. J. Physiol. Heart Circ. Physiol.* 278, H1671–H1678.